Simulating the 20 May 2013 Moore, Oklahoma tornado with a 100-metre grid-length NWP model

ATMOSPHERIC SCIENCE LETTERS
Atmos. Sci. Let. **17**: 453–461 (2016)
Published online 20 July 2016 in Wiley Online Library
(wileyonlinelibrary.com) **DOI:** 10.1002/asl.678

RMetS
Royal Meteorological Society

Simulating the 20 May 2013 Moore, Oklahoma tornado with a 100-metre grid-length NWP model

Kirsty E. Hanley,[1]* Andrew I. Barrett[2] and Humphrey W. Lean[1]
[1]*MetOffice@Reading, University of Reading, Reading, UK*
[2]*Department of Meteorology, University of Reading, Reading, UK*

**Correspondence to:*
K. E. Hanley, MetOffice@Reading, University of Reading, Meteorology Building, Reading RG6 6BB, UK.
E-mail: kirsty.hanley@metoffice.gov.uk

Received: 24 November 2015
Revised: 21 April 2016
Accepted: 6 June 2016

Abstract

Since 2013, the Met Office have run a 2.2 km horizontal gridlength version of the Unified Model (MetUM) as part of the National Oceanographic and Atmospheric Administration's Hazardous Weather Testbed Spring Forecasting Experiment. In this study, we perform high resolution MetUM simulations of the 20 May 2013 Oklahoma tornado outbreak at horizontal gridlengths between 2.2 km and 100 m. Here we present results showing that at 2.2 km gridlength the MetUM is able to simulate supercell-like storms whereas at O(100 m) gridlength it is able to simulate realistic-looking supercells with tornado-like vortices. This opens up the opportunity for using such simulations to highlight areas of enhanced tornado risk ahead of time.

Keywords: **tornado; Unified Model; 100-metre grid length**

1. Introduction

Accurate forecasting of severe thunderstorms is crucially important for providing spatially and temporally correct warnings of the convective-scale hazards they can cause, e.g. squall lines and tornadoes. In recent decades, the lead time for tornado warnings has greatly improved and currently averages at about 14 min (Wurman *et al.*, 2012). However, all of the National Oceanographic and Atmospheric Administration's (NOAA's) National Weather Service (NWS) tornado warnings are based upon detection by observers or the presence of a tornado vortex signature in radar data (Brotzge and Donner, 2013) meaning that the threat has to exist before a warning is issued, which limits further improvements in lead time unless an alternative method is found to warn before the threat exists.

Many operational weather centres, including the Met Office, now run order 1 km gridlength models for short-range weather forecasting. Although such models yield qualitatively more realistic precipitation fields than lower resolution simulations with parameterised convection (e.g. Kain *et al.*, 2008; Lean *et al.*, 2008; Weisman *et al.*, 2008; Schwartz *et al.*, 2009; Kendon *et al.*, 2012), these gridlengths are still unable to fully resolve the individual convective elements (e.g. Bryan *et al.*, 2003). As a result, we would not expect kilometre-scale models to be able to resolve tornadoes, however, they may be able to provide accurate short-term predictions of the storms that produce them.

As model gridlengths are decreased further to order 100 m, we may expect to start resolving features such as tornadoes. Although such gridlength simulations are currently unfeasible to run operationally, they can provide useful insight into tornado dynamics and demonstrate the added benefits of high resolution forecasts. There have been many idealized modelling studies of supercell and tornado dynamics (e.g. Wicker and Wilhelmson, 1995; Markowski *et al.*, 2003; Markowski and Richardson, 2014b; Orf *et al.*, 2014); however, there are few high resolution numerical studies based on real tornadic storms. One such study by Schenkman *et al.* (2014), simulated the 8 May 2003 Oklahoma City supercell using the Advanced Regional Prediction System (ARPS) with four one-way nested grids of 9 km, 1 km, 100 m and 50 m horizontal grid spacing. The 1 km simulation had a 5-min data assimilation cycle performed over a 70-min period, assimilating radar reflectivity and radial velocity from the Weather Surveillance Radar-1988 Doppler (WSR-88D) at Twin Lakes (KTLX) Oklahoma City. The 60-min, 100-m simulation obtained its initial conditions from the 1 km final analysis while the 40-min, 50-m gridlength simulation was nested within the 100 m simulation and obtained its initial conditions from the 100 m forecast

at 20 min. Tornado-like vortices were simulated in both the 100 and 50 m simulations: 30 min after the 100-m model was initialised and 10 min after the 50-m run was initialised. The timing, location and intensity of these vortices agreed well with the observed tornado. Previously, Mashiko *et al.* (2009) were able to produce a tornado-like vortex in a 26-min 50-m gridlength simulation of Typhoon Shanshan using the Japan Meteorological Agency Nonhydrostatic Model. The 50-m simulation was nested within a 5 km simulation, the initial conditions for which were provided by an operational regional analysis. Unlike Schenkman *et al.* (2014), no radar data were assimilated; however, the 50-m gridlength simulation was very short and would not aid real-time forecasting and warning of this storm.

In this article, we perform high resolution simulations of the 20 May 2013 tornado outbreak in Moore, Oklahoma using the Met Office Unified Model (MetUM) nested down to 100 m gridlength. Previously, 100 m gridlength versions of the MetUM have been used to study cold pooling in valleys (Vosper *et al.*, 2013), marine stratocumulus (Boutle *et al.*, 2014) and UK convection (Stein *et al.*, 2014; Hanley *et al.*, 2015). The main aim here is to investigate whether an order 100 m gridlength simulation, down-scaled from a free-running 2.2 km gridlength Numerical Weather Prediction (NWP) simulation, can resolve tornado-like vortices and potentially identify enhanced risk regions where tornadoes may occur many hours in advance of what could be obtained if assimilating radar data in the driving model. To our knowledge, this is the first study to simulate a tornado-like vortex over the US Great Plains in a high resolution NWP model at several hours lead-time.

2. Case overview

A 3-day stretch of severe weather across the Great Plains from 18–20 May 2013 produced the most deadly and devastating tornado of the year in the United States on 20 May affecting Moore, Oklahoma. Several supercell thunderstorms developed during early afternoon on 20 May 2013 in central Oklahoma. One of these supercells developed about 50 km southwest of Oklahoma City just after 1900 UTC and rapidly intensified, producing a tornado which touched down at 1956 UTC on the west side of Newcastle, Oklahoma (Atkins *et al.*, 2014). The tornado persisted for about 40 min and produced widespread enhanced-Fujita (EF) scale 3 damage, with localized EF4 and EF5 damage (Figure S1(b), Supporting Information). Several other, less intense, tornadoes were reported during the afternoon. A more detailed overview of the event and the accompanying synoptic conditions was given by Zhang *et al.* (2015).

3. Model description

The experiments are performed using version 8.2 of the MetUM. The MetUM solves non-hydrostatic, deep-atmosphere dynamics using a numerical scheme, which is semi-implicit and semi-Lagrangian (Davies *et al.*, 2005). The model uses Arakawa C-grid staggering in the horizontal and a terrain-following hybrid-height Charney–Phillips vertical grid. The model uses a comprehensive set of parameterisations including surface (Best *et al.*, 2011), mixed-phase cloud microphysics (Wilson and Ballard, 1999) and boundary-layer (Lock *et al.*, 2000). The model also includes a convection scheme (Gregory and Rowntree, 1990), although this is switched off at gridlengths below 4 km. Gridlengths of 2.2 km and finer also use a stability-dependent Smagorinsky-type subgrid turbulence scheme.

During the 2013 NOAA Hazardous Weather Testbed experiment, the Met Office was routinely running both a 4.4 and 2.2 km model (Clark *et al.*, 2014; Kain *et al.*, 2016). The 4.4 km model (US4) was one-way nested within the Met Office global model and covers the Contiguous United States (CONUS). The initial and boundary data for this domain were provided by the 0000 UTC Global analysis and forecast. The 2.2 km model (US2) was one-way nested within the US4 and covers most of the CONUS area. Both domains have 70 vertical levels, with the top at 40 km. The global model uses a hybrid incremental 4D-Var data assimilation system, no further data assimilation was performed on the limited area grids. The setup of the US4 and US2 domains was the same as the Met Office operational European 4 km model and UK 1.5 km model (UKV), respectively.

In this study, a suite of models were one-way nested within the US2 with horizontal gridlengths of 500, 200 and 100 m (Figure S1). The US2 gets its initial conditions and boundary data from the 20 May 2013 US4 model run and is initialised at 0300 UTC. The specification of the 500, 200 and 100 m models hereafter referred to as the 'nested models' is presented in Table 1. All models were integrated forward until 0000 UTC (21 h for the US2, 18 h for the 500 m model, 12 h for the 200 m model and 9 h for the 100 m model). The initialisation times were chosen to be at least 3 h ahead of when convection initiated in reality to allow the storms to develop within each domain.

The nested models configuration is based on the high resolution MetUM simulations performed by Hanley *et al.* (2015) and is very similar to the operational UKV and US2, but with a few differences. Unlike the US2, the

Table 1. Domain details and experimental setup.

Name	Grid length/ km	Domain size	Levels	Start time/ UTC	Time step/s	Convection scheme?
US4	4.4	CONUS	70	0000	100	Yes
US2	2.2	3740 × 2640 km	70	0300	75	No
500 m	0.5	600 × 500 km	140	0600	10	No
200 m	0.2	300 × 300 km	140	1200	6	No
100 m	0.1	150 × 150 km	140	1500	3	No

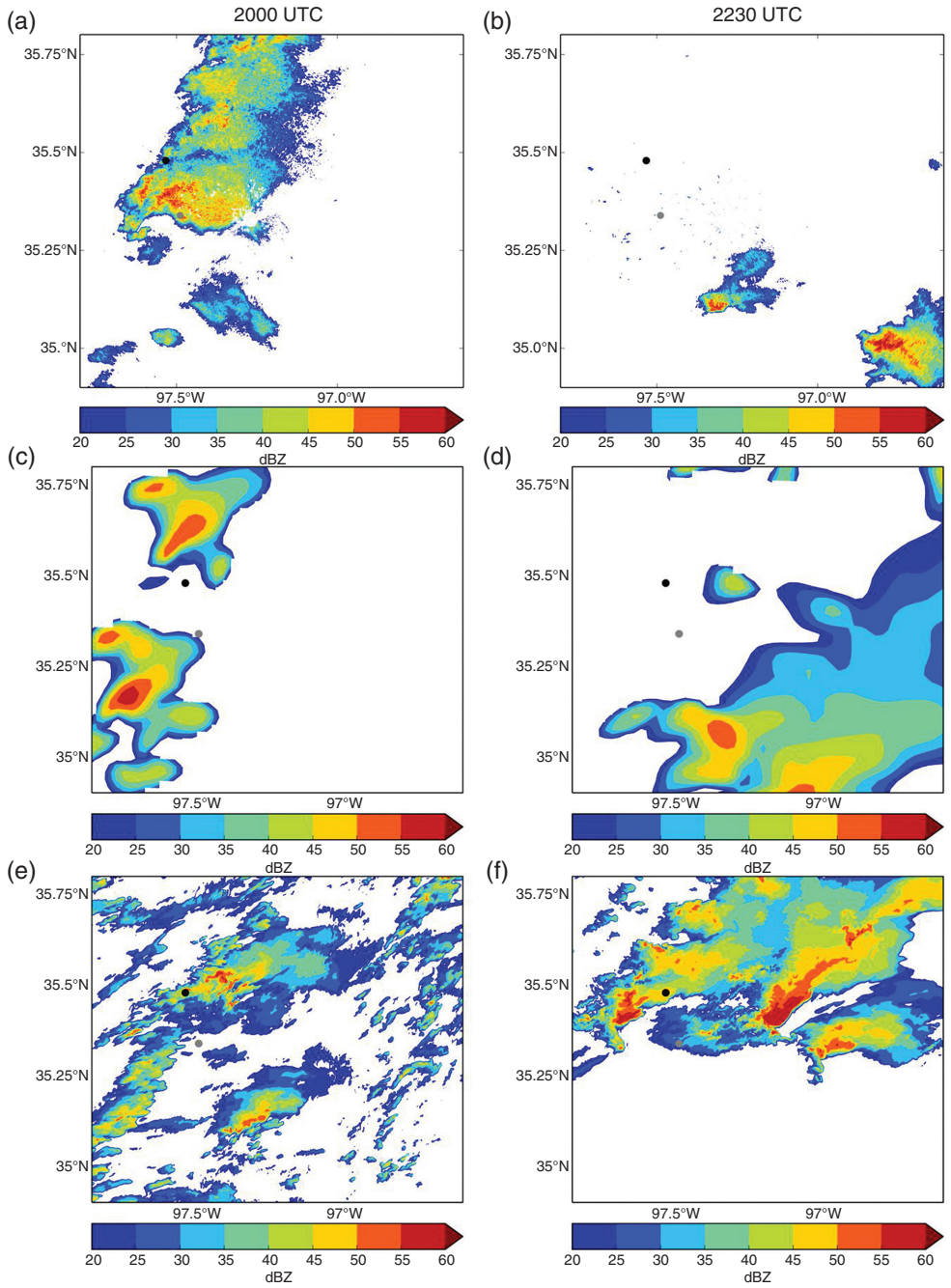

Figure 1. Reflectivity in dBZ at 2000 UTC (left) and 2230 UTC (right) 20 May 2013 from (a) and (b) the WSR-88D Twin Lakes, Oklahoma (KTLX) radar at an elevation angle of 0.5 degrees, (c) and (d) the 2.2 km model and (e) and (f) the 100 m model. The black and grey circles show the locations of Oklahoma City and Moore, respectively.

nested models have 140 vertical levels (corresponding to a spacing of ~75 m at 1 km above ground level compared to 150 m in the US2). Another difference between the models is the critical relative humidity (RH_{crit}) profile used for cloud formation. On the assumption that the subgrid variability of humidity is reduced in smaller grid boxes, the nested models use a larger RH_{crit} than the US2. The final difference of note is that the US2 uses the Smagorinsky subgrid mixing scheme only in the horizontal with vertical mixing done by the boundary layer scheme, whereas the higher resolution models apply the subgrid mixing scheme in both the horizontal and the vertical.

4. Simulation results

In this section, we begin by providing an overview of the 20 May 2013 Oklahoma supercells in the US2 and 100 m simulation. We then provide an analysis of the dynamics of the 200 and 100 m simulations at the tornado-scale, as they both produce tornado-like vortices.

4.1. Storm-scale overview

The MetUM provides surface precipitation rates as a diagnostic. The simulated surface reflectivity, Z, has

Atmospheric Science Letters published by John Wiley & Sons Ltd on behalf of the Royal Meteorological Society.

been derived from the surface rainrate, R, by assuming a Z–R relationship of $Z = 300R^{1.5}$. Figure 1 shows the simulated reflectivity from the US2 and the 100 m model compared with the WSR-88D KTLX radar reflectivity at 2000 and 2230 UTC. On this day, the US2 has convection initiating in the Oklahoma City region at about 1830 UTC (not shown) consistent with radar observations. The 100 m simulation initiates convection earlier but produces wide-spread light rain for several hours before organizing into larger cells by about 2000 UTC (Figure 1(e)). The US2 produces large cells that display some classic supercell features with high reflectivity cores and larger regions of low reflectivity on the forward-flank downdraft (FFD, Figure 1(c)). The size of the cells and the distribution of reflectivity compare reasonably well with the observed radar reflectivity; however, the cells in the US2 tend to be more circular than the observations. The 100 m simulation produces more realistic-looking supercells, at 2000 UTC the location of the Moore supercell is better represented by the 100 m simulation (Figure 1(e)). However, the 100 m simulation is producing too much widespread precipitation at this time and the supercell does not have a hook-echo feature suggesting it isn't tornadic. By 2230 UTC, the precipitation in the vicinity of Oklahoma City has decayed (Figure 1(b)); however, both the US2 and the 100 m simulation are still producing substantial precipitation. At this time, the supercells in the 100 m simulation each have a well-defined hook-echo (Figure 1(f)).

The hook echos in the 100 m simulation develop about 2.5 h later than the Moore tornado. Kilometre-scale ensemble simulations of this case with the WRF-ARW model by Zhang *et al.* (2015) showed that both the timing and location of the supercells were highly sensitive to small changes in synoptic conditions, so small timing and/or positional errors in the position of the dryline in the driving model could have led to the timing errors seen here in the 100 m simulation.

Downdrafts (rather than updrafts) are considered important in generating near-surface vertical vorticity by transporting vertical vorticity from mid-levels to the surface (e.g. Rotunno and Klemp, 1985; Markowski and Richardson, 2009; Kosiba *et al.*, 2013; Dahl *et al.*, 2014; Markowski and Richardson, 2014b; Naylor and Gilmore, 2014). Due to the deep-layer wind shear and upper-level winds, the bulk of the hydrometeors in a supercell is deposited on the forward flank of the main updraft. Evaporation of rain and melting and sublimation of ice lead to negative buoyancy in this region and the development of a FFD. The FFD in the US2 simulation is coincident with the main area of precipitation (Figure S2). A rear-flank downdraft (RFD) develops when the mesocyclone wraps precipitation around the updraft into drier air at the rear of the storm, leading to latent cooling (e.g. Lemon and Doswell, 1979). The RFD is not well resolved by the US2. Descending air within the RFD can tilt horizontal vorticity into the vertical and advect it towards the ground, leading to vertical vorticity near the ground (e.g. Davies-Jones and Brooks, 1993; Adlerman *et al.*, 1999). Numerical

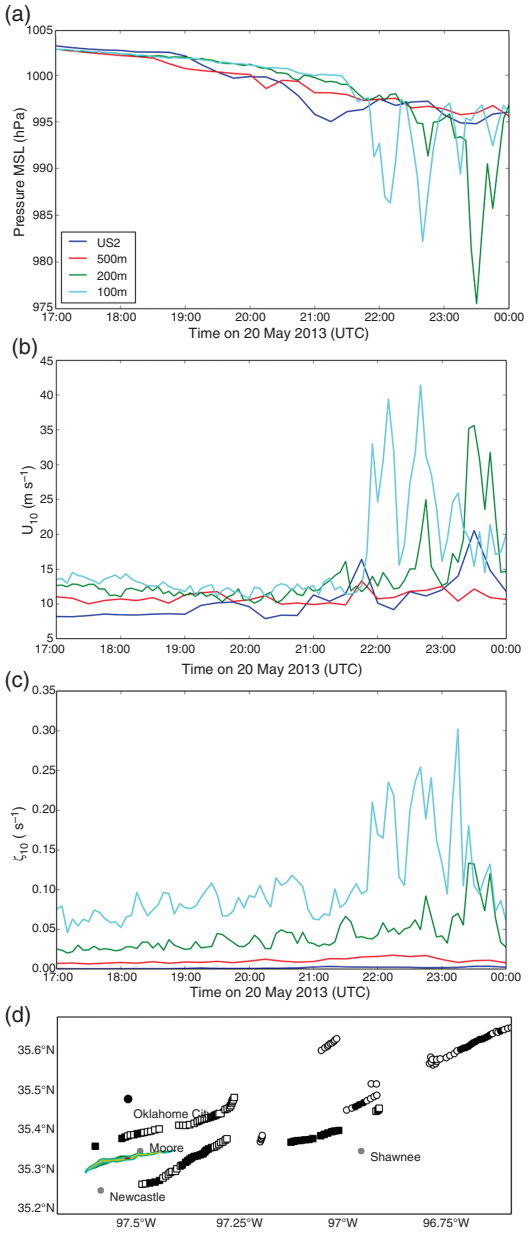

Figure 2. (a) Minimum mean sea level pressure in hPa, (b) maximum 10 m wind speed in m s^{-1} and (c) maximum 10 m vertical vorticity in s^{-1} for the US2 (blue), 500 m (red), 200 m (green) and 100 m (cyan) simulations of 20 May 2013. All data have been sampled over the region of the 100 m domain and is every 5 min. (d) Observed tornado damage path (filled contour) obtained from http://www.srh.noaa.gov/oun/?n=events-20130520 compared with location of maximum 10 m vorticity from the 200 m (circles) and 100 m (squares) simulations. White symbols indicate where the maximum 10 m wind is between 15 and 30 m s^{-1} and black symbols indicate where the maximum 10 m wind exceeds 30 m s^{-1}. Model data are every minute.

simulations of tornadoes by Wicker and Wilhelmson (1995) first indicated that some of the air parcels entering the tornado had indeed passed through the RFD. Most supercells develop near-ground rotation; however, fewer than 20% of supercells produce a tornado (Markowski and Richardson, 2014a). The lack of a RFD and a hook-echo in the US2 simulation may indicate that the gridlength is not sufficient to resolve the mesocyclone and therefore the simulated storm fails to

produce a RFD required for tornadogenesis. In the following section, we take a closer look at the 100 m simulation to determine whether the simulated hook-echo features are associated with tornado-like vortices.

4.2. Tornado-scale overview

The 100 and 200 m gridlength simulations both produce tornado-like vortices. The 500 m and US2 simulation both produce supercells, but do not produce tornado-like vortices. Tornado-like vortices were identified from rapid decreases of 10–20 hPa in the minimum mean sea level pressure (mslp) within the domain (Figure 2(a)) for both the 100 and 200 m simulations. The rapid pressure drops are coincident with increases of 10-m wind speed (Figure 2(b)) and 10-m vertical vorticity (Figure 2(c)). These vortices at 2230 UTC (and at other times, not shown) coincide with well-defined hook-echo structures in the surface reflectivity (Figure 1(f)), indicating that both 100 and 200 m simulations are producing tornado-like vortices. Similar rapid drops in pressure are not seen in the US2 and 500 m simulations, because these relatively-coarse gridlengths are not fine enough to resolve tornado-like vortices.

The vortices in both 100 and 200 m simulations have 10-m wind speeds exceeding 30 m s^{-1} that persist for at least 15 min (Figure 2(b)). Both models simulate tornadoes later in the day than the observed EF5 tornado but the 100 m simulation produced a vortex earlier than the 200 m simulation, potentially showing a benefit of better resolving the small-scale features. The 100 m simulation produces a stronger tornado-like vortex than the 200 m simulation. The 100 m simulation has a maximum 10 m wind speed of over 40 m s^{-1} whereas the 200 m simulation has a maximum of just over 35 m s^{-1}. The simulated strength of the tornado-like vortices is significantly weaker than the observed EF5 tornado; this is most likely due to insufficient resolution as the effective resolution of the MetUM is

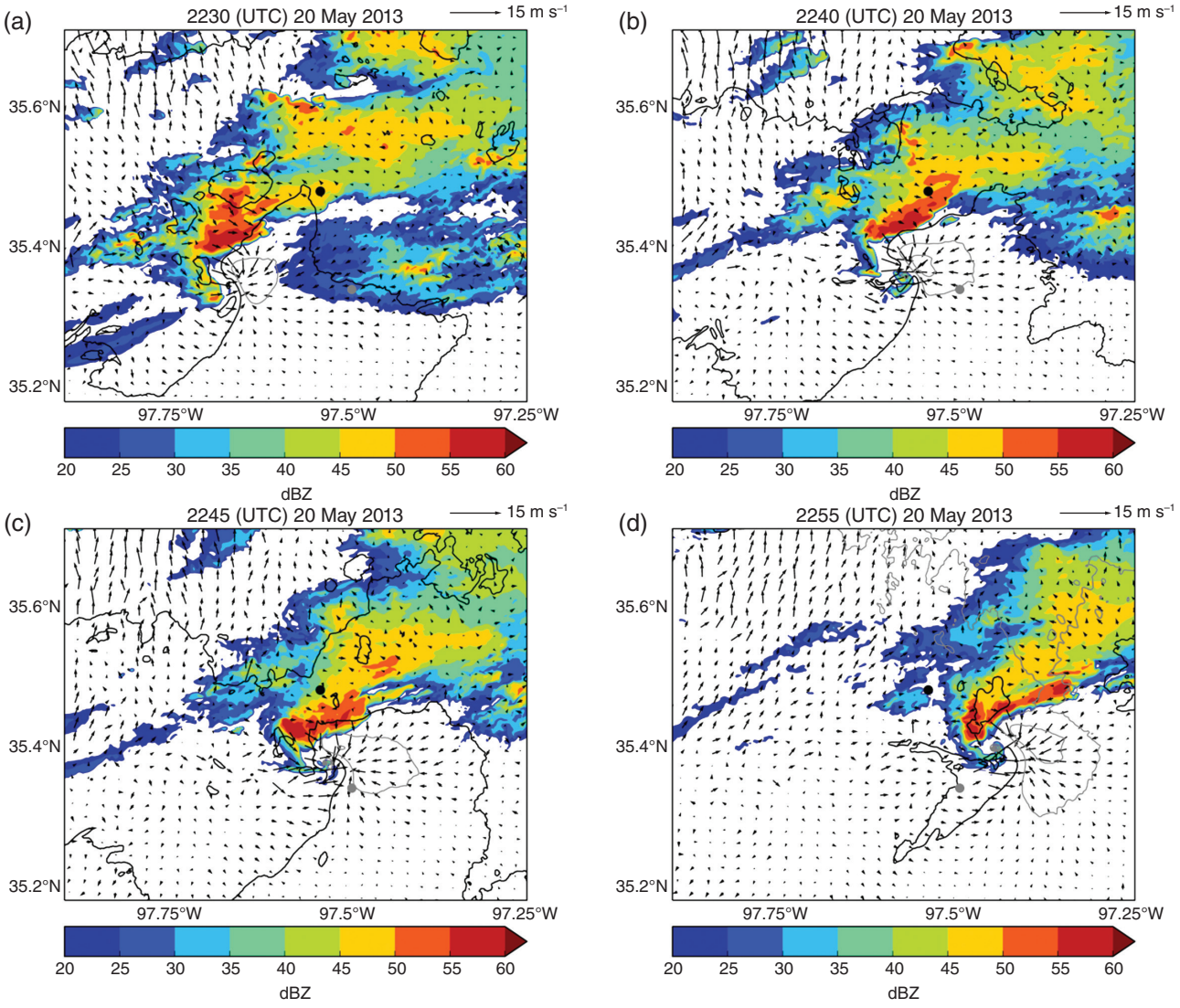

Figure 3. Simulated surface reflectivity in dBZ from the 100 m simulation at (a) 2230, (b) 2240, (c) 2245 and (d) 2255 UTC 20 May 2013. Vectors show the 10 m wind in m s^{-1}, grey contours depict mslp below 1000 hPa and black contours depict mslp above 1000 hPa with a contour interval of 1 hPa. The black and grey circles show the locations of Oklahoma City and Moore respectively.

several gridlengths. The simulated location, direction and length of the tornado paths are very similar to the observed tornado (Figure 2(d)). The points marked show the location of the 10 m vorticity maxima where the 10 m wind speed exceeded 15 m s^{-1}. The 100 m simulation produces two tornado-like vortices within 10 km of the observed EF5 tornado track. These two tornado-like vortices persist for about 40 min and both produce wind speeds exceeding 30 m s^{-1} (reflectivity shown in Figure 3). A third vortex occurs to the east of the observed EF5 tornado (see Figure 1(f)) and persists for about 15 min. The 200 m model also simulates two tornado-like vortices, both of which exceed 30 m s^{-1}. The first persists for about 10 min and the second persists for over 30 min. Both of these tornado-like vortices occur about 50 km further east, in Lincoln County, where an EF0 tornado was reported on this day. Although the model produces a tornado-like vortex with good agreement with the Moore tornado, Figure 2 shows some differences from the actual event itself with several tornado-like vortices occurring (white and black symbol tracks in Figure 2(d)). This reflects some challenges for tornado-scale forecasting in the future. While the model may produce some tornado-like vortices in the correct location, it may resolve tornado-like vortices that do not occur (or at least were not reported). Thus, providing tornado warnings based on these simulations may increase the warning lead time, however, the false alarm rate could also increase. It may be more valuable to use similar simulations to discriminate between tornadic and non-tornadic storm environments.

Figure 3 focuses on the supercell in the 100 m simulation nearest Moore, which produces an EF1 intensity tornado-like vortex. At 2230 UTC, the hook echo begins to form (Figure 3(a)); at this time a dynamically induced low pressure is present in the inflow region. By 2240 UTC (Figure 3(b)), the hook echo is well established and the dynamic low has deepened. During the next 5 min, the hook echo structure becomes more clearly defined (Figure 3(c)) but also the leading edge of the cold outflow (marked by the black 1000-hPa contour line to the south of the storm) from the RFD starts to separate the storm inflow from the updraft. By 2255 UTC (Figure 3(d)), the hook is quite tightly wrapped and well defined, but the cold outflow from the RFD is running ahead of the hook echo and cutting the storm off from the inflow. Ultimately the tornado-like vortex decays at this time, but the storm forms another tornado-like vortex later on as seen by the break in the tornado path in Figure 2(d) north-east of Moore.

Figure 4(a) shows vertical velocity at 1 km agl from the 100 m simulation at 2230 UTC. There is a strong updraft located near the hook-echo. The updraft is much stronger in the 100 m simulation than the US2 simulation as a result of it being better resolved. There is also a strong RFD in the hook-echo region and a weaker, larger area of downdrafts in the forward-flank region. Figure 4(b) shows a vertical cross-section through the main updraft and RFD from the 100 m simulation at the same time, 2230 UTC. At this time, a funnel cloud has developed which reaches down to the surface. Looking at the meridional wind component along the same cross-section (Figure 4(c)) shows that the updraft is associated with a wide area of rotation at mid-levels. At lower levels there is rotation coincident with the funnel cloud.

Within the same synoptic environment considered favourable for tornadoes, both tornadic and non-tornadic supercells occur. The reasons why one supercell produces a tornado and another does not are poorly understood. Markowski and Richardson (2009) suggest that tornadogenesis in supercells is a Goldilocks problem whereby the air feeding into the tornado has to be just the right temperature. Downdrafts and their accompanying negative buoyancy are crucial for baroclinic generation of vorticity, but excessive negative buoyancy can prevent near-surface parcels from being dynamically lifted, preventing tornadogenesis. One advantage of having a fairly long simulation is that there are multiple supercells simulated by the 100 m model. In a follow-on study we plan to compare the thermodynamic structure of the tornadic supercells with the non-tornadic supercells. The ability to use such forecasts to discriminate between tornadic and non-tornadic supercells may help reduce the high false alarm rate for both tornado warnings and tornado watches.

5. Discussion

In this study, we have performed high resolution simulations of the 20 May 2013 tornado outbreak. By nesting down to O(100 m) gridlength, the simulated supercells become more realistic and tornado-like vortices are produced. To our knowledge, this is the first time that tornado-like vortices have been simulated for a real tornado event at several hours lead time and without the use of high resolution data assimilation to force realistic storm development.

These simulations were performed with multiple nesting from the global model down to the 100 m simulation. Data assimilation was only performed on the global domain. Despite the lack of data assimilation, the model was able to simulate a tornado-like vortex within 50 km of the observed Moore tornado, albeit 2 h late. The demonstration here that sufficiently high-resolution simulations can resolve both supercells and tornado-like vortices, without requiring strong constraint from high-resolution radar data assimilation, is encouraging. By improving initial conditions using data assimilation on the limited area domains, there exists a real possibility of using similar high-resolution simulations to provide skilful forecasts that could result in longer-lead-time warnings of severe convective weather, or the ability to discriminate between tornadic and non-tornadic storm environments.

The tornado-like vortices in the 200 and 100 m gridlength simulations were identified from rapid decreases in minimum mslp of the order 10 hPa and were confirmed by the presence of a condensation

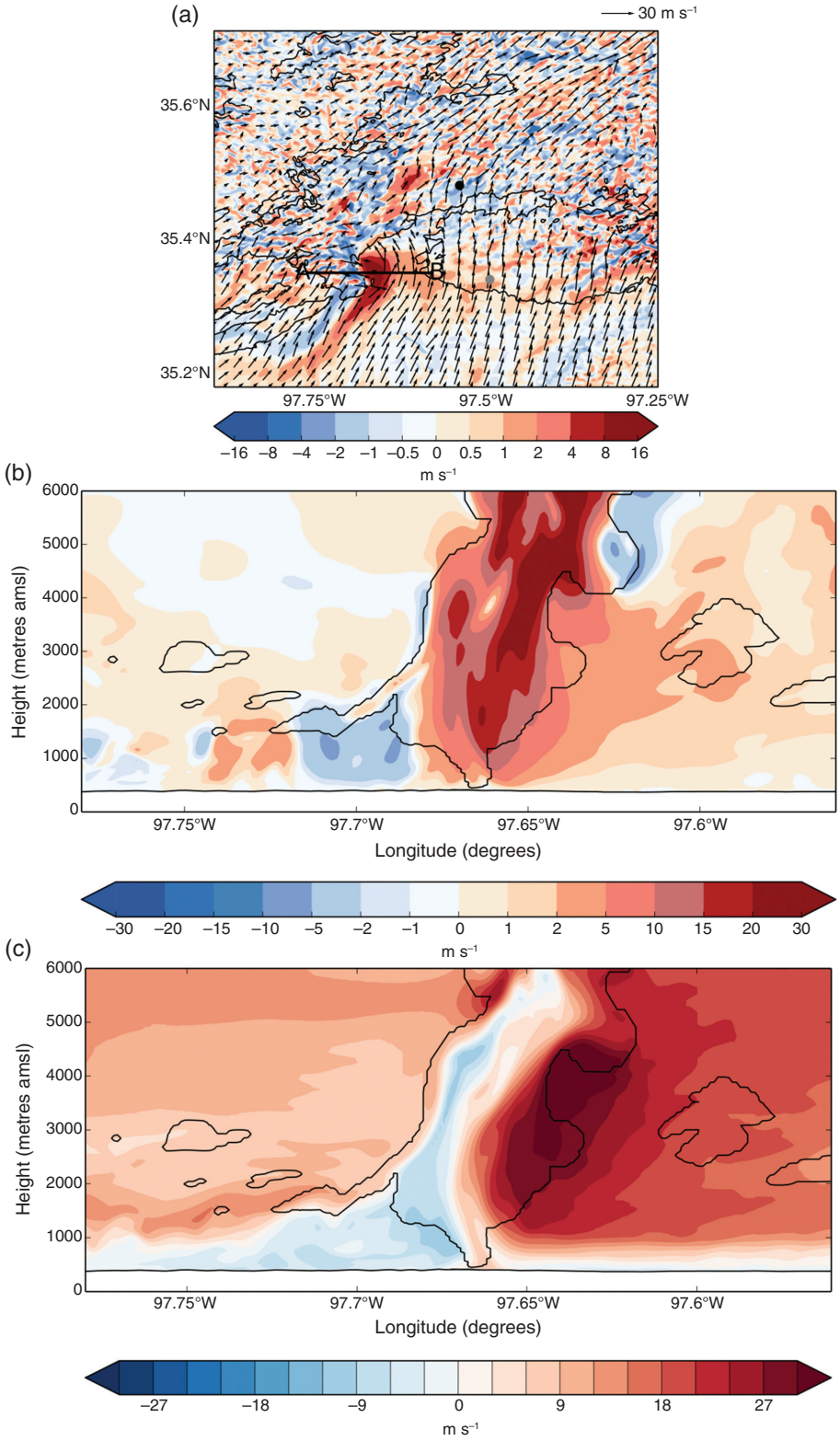

Figure 4. (a) Vertical velocity and wind vectors at 1 km agl in m s^{-1}. (b) Vertical velocity in m s^{-1} and (c) meridional wind component in m s^{-1} along 35.35°N (line A–B in (a)). All from the 100 m simulation at 2230 UTC on 20 May 2013. The black contours in (a) show surface reflectivity of 20 dBZ and the contours in (b) and (c) depict cloud water exceeding 0.001 g kg^{-1}.

funnel reaching down to the surface. Similar experiments were conducted on two further severe weather outbreaks from 2013: 30 and 31 May. On 30 May 2013, there were supercells across Oklahoma but no reported tornadoes; whereas, on 31 May 2013, the widest tornado in recorded history occurred in central Oklahoma. For both cases, the MetUM did a good job at capturing the supercellular features (not shown). Timeseries analysis similar to Figure 2 showed that for the 31 May 2013, both the 200 and 100 m gridlength

simulations produced tornado-like vortices similar in magnitude to those produced in the 20 May 2013 simulations; whereas, on 30 May 2013, no such vortices were simulated. This indicates that the MetUM potentially has some skill in discriminating between tornadic and non-tornadic supercells.

Although the tornado-like vortices simulated by the 200 and 100 m models look realistic, there are issues with the timing and location. This is to be expected because atmospheric predictability at the convective storm scale is limited, which presents some challenges in tornado-scale forecasting in the future. In particular, the model produces several tornado-like vortices in locations where tornadoes were not reported which could lead to increased false alarm rates. One technique for overcoming this uncertainty would be to run an ensemble of 100 m simulations nested within a kilometre-scale ensemble. However, this would be very computationally expensive. A cheaper alternative would be to use the kilometre-scale ensemble to determine the spatial and temporal uncertainty of supercells and then nest one or two 100 m simulations within the ensemble to determine the likelihood of the supercells being tornadic.

NOAA's National Weather Service is moving towards using order 1 km gridlength NWP models in so-called 'warn-on-forecasts' (Stensrud *et al.*, 2013). Although these gridlengths cannot resolve tornadoes, diagnostics such as mid-level updraft helicity and low-level shear are useful for identifying the mid-level rotation associated with supercell storms and previous studies have shown some skill in using updraft helicity to forecast tornado path lengths (Clark *et al.*, 2012, 2013). However, since only a small fraction of supercells actually produce tornadoes, it is not possible to forecast a tornado based on these diagnostics alone. In contrast, we showed in Section 4 that order 100 m NWP models can resolve tornado-like vortices, provided the tornado has a diameter of several gridlengths or greater. This means a relatively small percentage of tornadoes in nature will be resolved in a 100 m NWP model (i.e. most tornadoes have diameters smaller than the effective resolution of the model). However, larger tornadoes are generally more damaging and arguably the most important to forecast (e.g. Brooks, 2004; Agee and Childs, 2014). Further investigation into the difference between the tornadic and non-tornadic supercells at this resolution may provide insight into which supercells in lower resolution simulations are most likely to produce tornadoes. The use of 100 m simulations in this fashion, or through use of real-time (ensemble) simulations, could help improve the prediction of tornado outbreaks by identifying enhanced risk regions where tornadoes may occur and help reduce the high false alarm rate of tornado warnings by discriminating between tornadic and non-tornadic events.

Acknowledgements

The authors would like to thank Mark Weeks for initially setting up the US4 and US2 and Mike Coniglio and Jimmy Correia Jr. for their help in obtaining and visualizing NEXRAD II data. Thanks must also go to Steve Willington for leading the Met Office's involvement in the NOAA Hazardous Weather Testbed.

Supporting information

The following supporting information is available:

Figure S1. (a) Model domains used. The dashed black line shows the outline of the US2, the red line shows the 500 m domain, the blue line shows the 200 m domain and the green line shows the 100 m domain. Coloured contours show the orography of the US2. (b) Orography of the 100 m domain with the observed tornado damage path overlaid (coloured contours) obtained from http://www.srh.noaa.gov/oun/?n=events-20130520.

Figure S2. (a) Updraft vertical velocity in m s^{-1} and wind vectors at 1 km agl and (b) updraft helicity in m^2 s^{-2} between 2 and 5 km from the US2 simulation at 2000 UTC on 20 May 2013. The contours depict surface reflectivity of 20 dBZ (grey) and 50 dBZ (black).

References

Adlerman EJ, Droegemeier KK, Davies-Jones R. 1999. A numerical simulation of cyclic mesocyclogenesis. *Journal of the Atmospheric Sciences* **56**: 2045–2069.

Agee E, Childs S. 2014. Adjustments in tornado counts, F-Scale intensity, and path width for assessing significant tornado destruction. *Journal of Applied Meteorology and Climatology* **53**: 1494–1505.

Atkins NT, Butler KM, Flynn KR, Wakimoto RM. 2014. An integrated damage, visual, and radar analysis of the 2013 Moore Oklahoma EF5 tornado. *Bulletin of the American Meteorological Society* **95**: 1549–1561, doi: 10.1175/BAMS-D-14-00033.1.

Best MJ, Pryor M, Clark DB, Rooney GG, Essery RLH, Menard CB, Edwards JM, Hendry MA, Porson A, Gedney N, Mercado LM, Sitch S, Blyth E, Boucher O, Cox PM, Grimmond CSB, Harding RJ. 2011. The Joint UK Land Environment Simulator (JULES), model description – part 1:energy and water fluxes. *Geoscientific Model Development* **4**: 677–699.

Boutle IA, Eyre JEJ, Lock AP. 2014. Seamless stratocumulus simulation across the turbulent gray zone. *Monthly Weather Review* **142**: 1556–1569, doi: 10.1175/MWR-D-13-00229.1.

Brooks HE. 2004. On the relationship of tornado path length and width to intensity. *Weather and Forecasting* **19**: 310–319.

Brotzge J, Donner W. 2013. The tornado warning process: a review of current research, challenges, and opportunities. *Bulletin of the American Meteorological Society* **94**: 1715–1733.

Bryan GH, Wyngaard JC, Fritsch JM. 2003. Resolution requirements for the simulation of deep convection. *Monthly Weather Review* **131**: 2394–2416.

Clark AJ, Kain JS, Marsh PT, Correia J Jr, Xue M, Kong F. 2012. Forecasting tornado pathlengths using a three-dimensional object identification algorithm applied to convection-allowing forecasts. *Weather and Forecasting* **27**: 1090–1113.

Clark AJ, Gao J, Marsh PT, Smith T, Kain JS, Correia J Jr, Xue M, Kong F. 2013. Forecasting tornado pathlengths using a three-dimensional object identification algorithm applied to convection-allowing forecasts. *Weather and Forecasting* **28**: 387–407.

Clark A, Willington S, Suri D, Kain JS, Coniglio MC, Knopfmeier KH, Weiss SJ, Jirak IL, Lean HW, Roberts R, Weeks M, Dean AR, Melick CJ, Karstens CD, Marsh PT, Correia J Jr. 2014. Comparing the NSSL-WRF Model and Convection-allowing Versions of UKMET's Unified Model during the 2013 and 2014 NOAA/HWT Spring Forecasting Experiments. In 27th Conference on Severe Local Storms. American Meteorological Society: Madison, WI.

Dahl JML, Parker MD, Wicker LJ. 2014. Imported and storm-generated near-ground vertical vorticity in a simulated supercell.

Journal of the Atmospheric Sciences **71**: 3027–3051, doi: 10.1175/JAS-D-13-0123.1.

Davies T, Cullen MJP, Malcolm AJ, Mawson MH, Staniforth A, White AA, Wood N. 2005. A new dynamical core for the Met Office's global and regional modelling of the atmosphere. *Quarterly Journal of the Royal Meteorological Society* **131**: 1759–1782.

Davies-Jones RP, Brooks H. 1993. Mesocyclogenesis from a theoretical perspective. In *The Tornado: Its Structure, Dynamics, Prediction and Hazards*. Church C, Burgess D, Doswell C, Davies-Jones R (eds). American Geophysical Union Press; Washington, DC; 105–114.

Gregory D, Rowntree PR. 1990. A mass flux convection scheme with representation of cloud ensemble characteristics and stability dependent closure. *Monthly Weather Review* **118**: 1483–1506.

Hanley KE, Plant RS, Stein THM, Hogan RJ, Nicol JC, Lean HW, Halliwell C, Clark PA. 2015. Mixing length controls on high resolution simulations of convective storms. *Quarterly Journal of the Royal Meteorological Society* **141**: 272–284, doi: 10.1002/qj.2356.

Kain JS, Weiss SJ, Bright DR, Baldwin ME, Levit JJ, Carbin GW, Schwartz CS, Weisman ML, Droegemeier K, Weber DB, Thomas KW. 2008. Some practical considerations regarding horizontal resolution in the first generation of operational convection-allowing NWP. *Weather and Forecasting* **23**: 931–952.

Kain JS, Clark AJ, Coniglio MC, Knopfmeier KH, Karstens CD, Willington S, Weeks M, Roberts NM, Lean HW, Wilkinson JM, Gilchrist L, Hanley KE, North R, Suri D, Weiss SJ, Jirak IL. 2016. Collaborative efforts between the U.S. and U.K. to advance prediction of high impact weather. *Bulletin of the American Meteorological Society*, in preparation.

Kendon EJ, Roberts NM, Senior CA, Roberts MJ. 2012. Realism of rainfall in a very high resolution regional climate model. *Journal of Climate* **25**: 5791–5806, doi: 10.1175/JCLI-D-11-00562.1.

Kosiba K, Wurman J, Richardson Y, Markowski P, Robinson P, Marquis J. 2013. Genesis of the Goshen County, Wyoming, tornado on 5 June 2009 during VORTEX2. *Monthly Weather Review* **141**: 1157–1181.

Lean HW, Clark PA, Dixon M, Roberts NM, Fitch A, Forbes R, Halliwell C. 2008. Characteristics of high-resolution versions of the Met Office Unified Model for forecasting convection over the United Kingdom. *Monthly Weather Review* **136**: 3408–3424, doi: 10.1175/2008MWR2332.1.

Lemon LR, Doswell CA. 1979. Severe thunderstorm evolution and mesocyclone structure as related to tornadogenesis. *Monthly Weather Review* **107**: 1184–1197.

Lock AP, Brown AR, Bush MR, Martin GM, Smith RNB. 2000. A new boundary layer mixing scheme. Part I: scheme description and single-column model tests. *Monthly Weather Review* **128**: 3187–3199.

Markowski PM, Richardson YP. 2009. Tornadogenesis: our current understanding, forecasting considerations, and questions to guide future research. *Atmospheric Research* **93**: 3–10.

Markowski P, Richardson Y. 2014a. What we know and don't know about tornado formation. *Physics Today* **67**: 26–31, doi: 10.1063/PT.3.2514.

Markowski PM, Richardson YP. 2014b. The influence of environmental low-level shear and cold pools on tornadogenesis: insights from idealized simulations. *Journal of the Atmospheric Sciences* **71**: 243–275, doi: 10.1175/JAS-D-13-0159.1.

Markowski PM, Straka JM, Rasmussen EN. 2003. Tornadogenesis resulting from the transport of circulation by a downdraft: Idealized numerical simulations. *Journal of the Atmospheric Sciences* **60**: 795–823.

Mashiko W, Niino H, Kato T. 2009. Numerical simulation of tornadogenesis in an outer-rainband minisupercell of Typhoon Shanshan on 17 September 2006. *Monthly Weather Review* **137**: 4238–4260, doi: 10.1175/2009MWR2959.1.

Naylor J, Gilmore MS. 2014. Vorticity evolution leading to tornadogenesis and tornadogenesis failure in simulated supercells. *Journal of the Atmospheric Sciences* **71**: 1201–1217.

Orf L, Wilhelmson R, Wicker L. 2014. Numerical simulation of a supercell with an embedded long-track EF5 tornado. Special Symposium on Severe Local Storms: The Current State of the Science and Understanding Impacts. American Meteorological Society, Atlanta, GA

Rotunno R, Klemp J. 1985. On the rotation and propagation of simulated supercell thunderstorms. *Journal of the Atmospheric Sciences* **42**: 271–292.

Schenkman AD, Xue M, Hu M. 2014. Tornadogenesis in a high-resolution simulation of the 8 May 2003 Oklahoma City supercell. *Journal of the Atmospheric Sciences* **71**: 130–154.

Schwartz CS, Kain JS, Weiss SJ, Xue M, Bright DR, Kong F, Thomas KW, Levit JJ, Coniglio MC. 2009. Next-day convection-allowing WRF model guidance: a second look at 2-km versus 4-km grid spacing. *Monthly Weather Review* **137**: 3351–3372.

Stein THM, Hogan RJ, Hanley KE, Clark PA, Halliwell C, Lean HW, Nicol J, Plant RS. 2014. The three-dimensional microphysical structure of convective storms over the southern United Kingdom. *Monthly Weather Review* **142**: 3264–3283, doi: 10.1175/MWR-D-13-00372.1.

Stensrud DJ, Wicker LJ, Xue M, Dawson II DT, Yussouf N, Wheatley DM, Thompson TE, Snook NA, Smith TM, Schenkman AD, Potvin CK, Mansell ER, Lei T, Kuhlman KM, Jung Y, Jones TA, Gao J, Coniglio MC, Brooks HE, Brewster KA. 2013. Progress and challenges with warn-on-forecast. *Atmospheric Research* **123**: 2–16.

Vosper S, Carter E, Lean H, Lock A, Clark P, Webster S. 2013. High resolution modelling of valley cold pools. *Atmospheric Science Letters* **14**: 193–199, doi: 10.1002/asl2.439.

Weisman ML, Davis C, Wang W, Manning KW, Klemp JB. 2008. Experiences with 0-36-h explicit convective forecasts with the WRF-ARW model. *Weather and Forecasting* **23**: 407–437.

Wicker LJ, Wilhelmson RB. 1995. Simulation and analysis of tornado development and decay within a three-dimensional supercell thunderstorm. *Journal of the Atmospheric Sciences* **52**: 2675–2703.

Wilson DR, Ballard SP. 1999. A microphysically based precipitation scheme for the UK Meteorological Office Unified Model. *Quarterly Journal of the Royal Meteorological Society* **125**: 1607–1636.

Wurman J, Dowell D, Richardson Y, Markowski P, Rasmussen E, Burgess D, Wicker L, Bluestein HB. 2012. The second verification of the origins of rotation in tornadoes experiment: VORTEX2. *Bulletin of the American Meteorological Society* **93**: 1147–1170.

Zhang Y, Zhang F, Stensrud DJ, Meng Z. 2015. Practical predictability of the 20 May 2013 tornadic thunderstorm event in Oklahoma: sensitivity to synoptic timing and topographical influence. *Monthly Weather Review* **143**: 2973–2997, doi: 10.1175/MWR-D-14-00394.1.